Research Square

Preprints are preliminary reports that have not undergone peer review.
They should not be considered conclusive, used to inform clinical practice,
or referenced by the media as validated information.

High-temperature thermal performance of ceramic-array load bearing multi- layer insulation for radioisotope thermophotovoltaic system

Rongyu Shao
Lanzhou University
Zhiyang Wang
Lanzhou University
Chengzhi Han
Beijing Institute of Spacecraft System Engineering
Aixiang Yang
yangax@lzu.edu.cn
Lanzhou University
Dingjun Zhu
Lanzhou University
Jianxiong Shao
Lanzhou University
Ximeng Chen
Lanzhou University

Research Article

Keywords: Radioisotope thermophotovoltaic system, Ceramic array Load Bearing multi-layer insulation, Insulation frame heat loss, Optical cavity size

Posted Date: November 16th, 2026

DOI: https://doi.org/10.21203/rs.3.rs-11239156/v1

License: This work is licensed under a Creative Commons Attribution 4.0 International License.
Read Full License

Additional Declarations: No competing interests reported.

High-temperature thermal performance of ceramic-array load bearing multi-layer insulation for radioisotope thermophotovoltaic system

Rongyu Shao[a,b], Zhiyang Wang[a,b], Chengzhi Han[c], Aixiang Yang[a,b,*], Dingjun Zhu[a,b], Jianxiong Shao[a,b,*], Ximeng Chen[a,b]

a MOE Frontiers Science Center for Rare Isotopes, Lanzhou University, Lanzhou 730000, China;

b School of Nuclear Science and Technology, Lanzhou University, Lanzhou 730000, China;

c Beijing Institute of Spacecraft System Engineering, Beijing 100190, China.

E-mail addresses: yangax@lzu.edu.cn, shaojx@lzu.edu.cn

Abstract

A hollow ZrO_2 ceramic array Load Bearing multi-layer insulation (LBMLI) is proposed for the radioactive thermophotovoltaic system (RTPV). Two theoretical models including the finite element model and layer-by-layer model are compared to analyze the thermal insulation performance. The number of layers, spacing, ceramic array quantity, thermal conductivity of spacing material, and reflective screen emissivity on heat loss are analyzed. At the LBMLI of 9 dots' ceramic array, as the quantity of layers increased from 15 to 20, the heat power loss significantly decreased from 22.5 W to 17 W. By reducing the emissivity from 0.1 to 0.025, the heat loss is almost linearly reduce to 8.5 W. For mechanical stability, a 15-layer-screen ceramic array LBMLI is designed for the present RTPV, with 25 ceramic arrays in each layer. When the input power is 250 W, if not considering insulation frame heat loss of the ceramic array LBMLI, the temperature at heat source center could reach 1106.3 ℃, and the thermal efficiency of ceramic array LBMLI is 69.5%. When it is considered, the temperature of the heat source is 1079.4 ℃, and $\eta_{thermal}$ is 57.0%. Moreover, considering optical cavity size, when reducing the lateral two dimensions of ceramic array LBMLI by 8 cm each, the temperature at heat source center changes to 1159.9 ℃ when considering insulation frame heat loss, with $\eta_{thermal}$ being 60.2%. Results show that hollow ZrO_2 ceramic array LBMLI is expected to reduce the heat leakage.

Keywords: Radioisotope thermophotovoltaic system; Ceramic array Load Bearing multi-layer insulation; Insulation frame heat loss; Optical cavity size.

1. Introduction

Many space missions' destinations are to places where solar power is impractical. Such location is either extremely far from the sun or persist in shadow for most of the orbital period. To meet the energy demands of these missions, several new power generation concepts utilize nuclear heat sources combined with thermal-to-electric converter method to produce the electric power[1]. Since the 1960s, NASA has deployed 42 radioisotope thermoelectric generators (RTGs) for electric power on 25 spacecraft[2].

RTG systems rely on decay heat released by radioactive plutonium-238 (Pu-238), which can be converted into electricity by using thermoelectric converters[3]. Nevertheless, RTGs suffer from an electric conversion efficiency below 10%[4]. Therefore, since 1990, NASA explored new thermoelectric technologies, including dynamic systems such as Stirling and Bretton cycles, and static systems such as radioisotope thermophotovoltaic (RTPV) systems and advanced thermoelectric (TE)[5].

In the RTPV systems, the conversion efficiency of the thermal-to-electric is highly dependent on the temperature of the emitter (>1000 °C) [6], and the thermal energy from the heat source (GPHS) is connected to emitters. At this temperature condition, TPV systems' efficiencies exceed 20%[7]. Increasing the heat source temperature enhances the electrical performance of the RTPV system, as the power density received by the PV cell increases accordingly[8]. However, in the past, studies on the emitter or filter have demonstrated highly promising results[9]. For the RTPV system, the cavity with higher heat insulation is important to transferred to the PV cells[2]. It is often composed by multi-layer thermal insulation (MLI), being designed to reduce both the conductive and radiative losses to the vacuum housing[10]. NASA designed 60 layers of 0.008 mm W/Mu foils separated by ZrO_2 spacer particles[11], and when using a 500W heat source, the canister (Mo/Re +W) as the emitter's temperature is 1034 ℃, but the MLI's thermal performance has not yet been thoroughly verified, and the matching connection between the MLI's screen edges and the heat sink structure was not provided. For these reasons, we propose a MLI's structure that possesses the ideal characteristics of efficiently reflecting spectral energy and a low thermal conductivity.

The MLI comprises low thermal conductivity spacers and high-reflective screens[12], and is the most efficient thermal insulation element[13]. At present, the research on MLI mainly includes structural optimization and the analysis of parameter influences. In terms of structural research, in 2022, Mengjun Chen et al. studied a composite thermal insulation material without interlayer contact space named carbon fiber materials and multi-layer thermal insulation (CFMLI), which has low thermal conductivity and thermal performance stability[14]. However, the interior of the fiber material is grid-like and has many pores, which makes it impossible to maintain precise layer spacing[15]. Meanwhile, the reflective screen in the fiber spacer material composite MLI have extensive contact with the fiber material, resulting in an increase in heat conduction loss caused by the contact between the reflective screen and the spacer material[16]. S.A. Dye et al. develop a novel Load Bearing multi-layer insulation (LBMLI) suitable of self-supporting thermal shields and having the high thermal performance, it uses the strength of discrete polymer spacers to control interlayer spacing and support the external load, but only suitable for application below 295 K[17]. In 2024, Xiaoqi Zhou et al. studied a small scale MLI fabricated at the micron-to-millimeter scale for ultrahigh temperature systems, which combines silica aerogel/TiN films and silica fiber/silicon wafer structures, using both field radiative heat transfer models. The MLI can retain 78% - 93% of the radiative heat at 1400 K, with a thickness only 24.5% - 36.8% of that of previously MLI materials[18]. As a result, existing high-temperature MLI designs are mostly oriented toward transient-heating protection for

hypersonic vehicles. They are not well-suited to the long-term steady high-temperature working conditions of the RTPV systems.

In terms of theoretical analysis, in 2014, Huang et al. adopted the finite element analysis model to establish a theoretical model combining radiative heat transfer and conductive heat transfer of high-temperature multi-layer insulation materials under pneumatic heating conditions, and analyzed the influence of multiple variables on the transient heat transfer performance of MLI[19]. In 2018, Chen et al. proposed the coupled heat conduction and heat radiation control equation[20]. The control equation was solved by using the finite volume method and the discrete coordinate method. Considering factors such as gas pressure, the density of fiber materials, the number of reflective foil layers, and the emissivity of the reflective foil comprehensively, the optimized structure of the composite MLI was studied. At present, the theoretical analysis of MLI is mainly based on the finite element analysis of the coupling process of heat conduction and heat radiation. Or the heat transfer process inside the MLI is superimposed and calculated. However, no study has conducted a detailed comparison of the results obtained by the above two calculation methods yet.

Given the recent strides in the related research, we propose a novel structure of LBMLI architecture featuring a hollow ZrO_2 cylindrical ceramic array, specifically designed for high-temperature environments. Results including the finite element model as well as layer-by-layer model are compared. Then, the influences of the number of the reflective screen, the thermal conductivity of spacer material, the number of the ceramic dots, the spacing between the reflective screens and the surface emissivity of the reflective screens are analyzed. A 15-layer ceramic array LBMLI is used in RTPV system, and its impact on the temperature of the system's heat source is calculated when the heat power increases. Additionally, the detailed thermal analysis results of edge heat loss effects and optical cavity size fully shows the importance of ceramic array LBMLI in the RTPV system. This work aims to bridge the existing research gap and to offer a dependable basis for the design and optimisation of high-temperature multilayer insulation in RTPV and related space power systems

2. Ceramic array LBMLI design methodology

2.1 Ceramic array LBMLI in the RTPV system

Most MLIs are composed of reflective screens and fibrous spacer materials, but the thermal performance is significantly affected by the contact area and contact pressure. When fibrous spacer materials are applied, the contact area is usually large and the spacing between the reflective screens can not been ensured. In this study, the ceramic array between the reflective screens has mechanical strength, ensuring that the spacing between adjacent reflective screens remains stable. For radioisotope thermophotovoltaic systems' applications[2], the edges of ceramic array LBMLI must also be specially sealed. As shown in Fig. 1, the present RTPV system's two end side faces are covered with ceramic array LBMLI, so the ceramic array LBMLI is in close and heat contact with the water cooling plate, and the other four side faces radiate heat

through spectrally selective filters to PV cells array, which are the insides of the cooling plate.

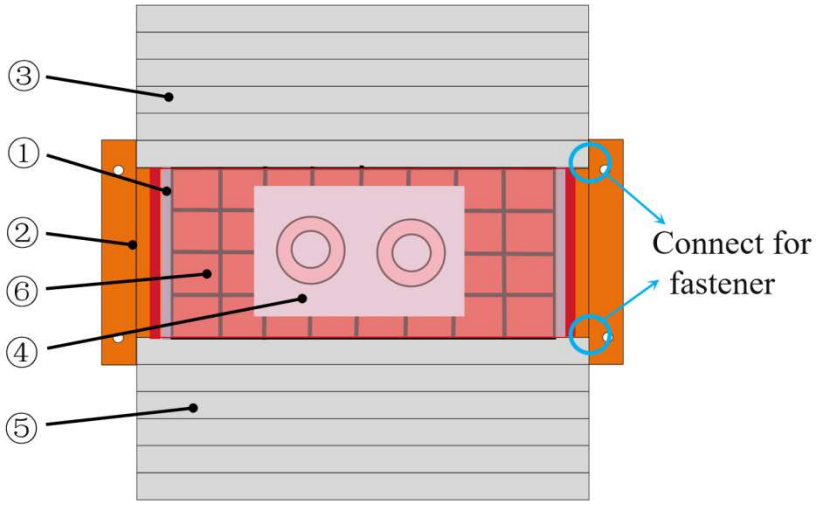


Fig. 1 RTPV system model: ① Filter; ② Cooling plate; ③ Ceramic array LBMLI at the top end; ④ Heat source; ⑤ Ceramic array LBMLI at the low end; ⑥ PV cells array

Based on the research of Schock[21], ZrO_2 particles spacing material is used to fill the gaps between the reflective screens. As shown in Fig. 2, ceramic array LBMLI consists of molybdenum metal reflective screens and hollow ZrO_2 ceramic array spacer materials, and the edges of the ceramic array LBMLI are sealed with aerogel frame. The ceramic array spacer material are closely bonded on the surface of the reflective screen by means of spraying[22]. Meanwhile, ceramic-array spacer layer has the advantages of easy to manufacture and high temperature resistance[23].

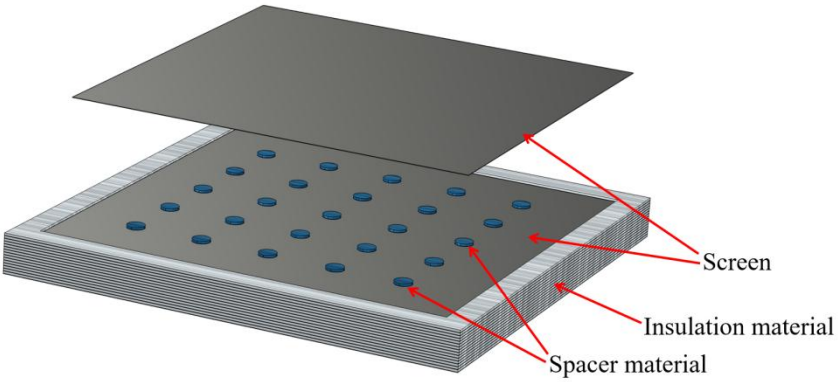


Fig. 2 Design of the ceramic array LBMLI

2.2 3D Numerical model

RTPV systems are usually applied in a vacuum environment, only the combined heat transfer process of heat radiation and heat conduction are considered in the ceramic array LBMLI.

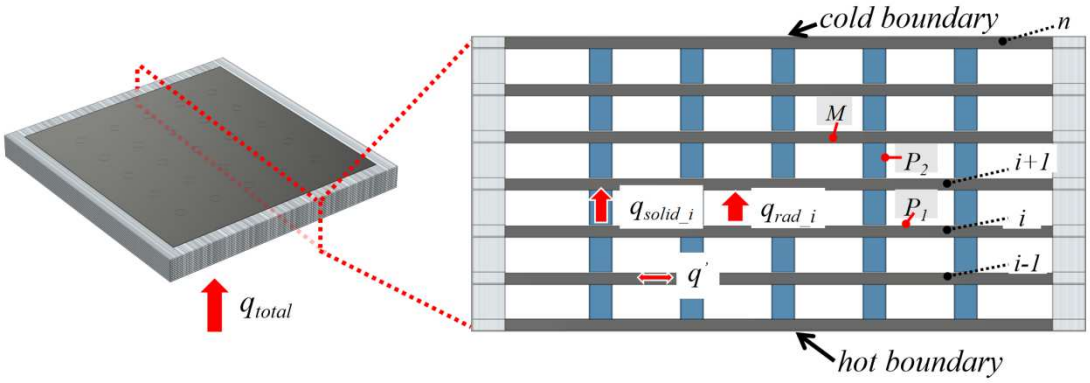


Fig. 3 Heat transfer process by numerical model

In Fig. 3, one end of the reflective screen is set as high temperature, which is named the hot boundary, because the side is close to the heat source, while the other end is lower temperature, which is named the cold boundary. Suppose there is no heat exchange at the frame of the ceramic array LBMLI, the heat transfer pathway within the ceramic array LBMLI include three types: thermal radiation (q_{rad}) between reflective screens, solid conduction (q_{solid}) through spacer materials, and solid conduction ($q^{'}$) occurring within the screens. For a ceramic array LBMLI composed of n layers of reflective screens, the temperature of the i-th layer of reflective screen is higher than the temperature of the $i + 1^{st}$ layer of reflective screen. Part of energy is emitted from the i^{th} layer of reflective screen to the surface of the $i + 1^{st}$ layer of reflective screen in the form of thermal radiation. The others energy is transferred in the form of heat conduction to surface of the $i + 1^{st}$ layer of the reflective screen[24]. Eventually, heat power fluxes from the hot boundary screen to the cold boundary screen of the entire ceramic array LBMLI's reflective screen.

At any time t, considering that there are no pores inside the spacer material and the reflective screen, and the thermal radiation heat transfer process within the material is not considered. For any position point M inside the spacer material or the reflective screen material, rather than in the point of any surface, according to the law of conservation of energy, it can be described as:

$$\rho C \frac{\partial T}{\partial t} = \frac{\partial}{\partial x}\left(k \frac{\partial T}{\partial x}\right) \tag{1}$$

where ρ is the density of the position, C is the specific heat capacity, k is the thermal conductivity, T is the temperature of the position point M.

At the boundary position of the non-contact area between the reflective screen surface inside the MLI and the spacer material, as shown in Fig. 3, energy transfer at point P_1 by the heat transfer process can be obtained as follows:

$$\rho_1 C_1 \frac{\partial T_1}{\partial t} = \frac{\partial}{\partial x}\left(k_1 \frac{\partial T_1}{\partial x}\right) - \frac{\partial q''_{r_P1}}{\partial x} \tag{2}$$

where q''_{r_P1} is the radiant heat flux generated by two adjacent screens of the MLI, k_1 is the thermal conductivity of the reflective foil material, ρ_1 is the density of the reflective

screen, C_1 is the heat capacity of the reflective screen, T_1 is the temperature at position P_1 of the reflective screen.

Suppose that for any layer screen, the temperature of its surface is exactly the same. Meanwhile, suppose the emissivity of any ceramic dot is ignored, because the areas of ceramic dot is very small compared the screen's area, and this approach is slightly higher than the actual. The thermal radiation from the ith layer of reflective screen's cold surface to the i + 1st layer of the reflective screen's hot surface can be expressed as:

$$q''_{r_i,\ i+1}=K_{r_i}(T_i - T_{i+1})Y_{i,\ i+1} \tag{3}$$

where $Y_{i,\ i+1}$ is defined as the fraction of radiant energy from the cold surface i of the reflective screen that towards to the hot surface screen i+1, named viewing angle coefficient. When the size of the reflective screen is infinitely large or the insulation material frame does not absorb heat, $Y_{i,\ i+1}$ is regarded as 1. T_i is the temperature of the i screen's cold surface, T_{i+1} is the temperature of the $i+1$ screen's hot surface, K_{r_i} is the radiation heat transfer coefficient:

$$K_{r_i}=[\sigma(T_i+T_{i+1})(T_i^2 + T_{i+1}^2)]/(\frac{1}{\varepsilon_i}+\frac{1}{\varepsilon_{i+1}}-1) \tag{4}$$

where, ε_i and ε_{i+1} are the emissivity of screens by i^{th} layer and the $i+1^{st}$ layer surfaces respectively. In the COMSOL software, K_{r_i} can usually be calculated.

For the surface of the ceramic dot inside the MLI, at the boundary position where it is not in contact with the reflective screen, as shown at position P_2 in Fig. 3, it can be concluded that:

$$\rho_2 C_2 \frac{\partial T_2}{\partial t}=\frac{\partial}{\partial x}\left(k_2 \frac{\partial T_2}{\partial x}\right) \tag{5}$$

where k_2 is the thermal conductivity of the ceramic dots spacer material, where ρ_2 is the density of the ceramic dots spacer material, C_2 is the heat capacity of the ceramic dots spacer material, T_2 is the temperature at position P_2.

The initial conditions and the boundary conditions of the hot boundary and cold boundary surfaces of the MLI are:

$$T(X,\ 0) = T_0 = 20\ ℃ \tag{6}$$

$$T(0,\ t) = T_1(t) \tag{7}$$

$$T(n,\ t) = T_n(t) \tag{8}$$

where X is any position of the reflective screen and the ceramic dots spacer material, n is the outer surface of the coldest boundary of the reflective screen, 0 is the initial state or initial position at time. The screens we selected and considered are molybdenum, for its stability at high temperature. Heat conduction and surface radiation for surface radiation are coupled in COMSOL software[25].

2.3 2D Layer-by-layer model

According to the definition of the layer-by-layer model, the heat flux inside the ceramic array LBMLI can be regarded as the sum of the radiant heat flux and the

conducted heat flux. Assumed that the thermal radiation and solid conduction are independent of each other[26]. Fig. 4 shows the heat transfer process, the heat conduction process inside the reflective screen is not taken into account.

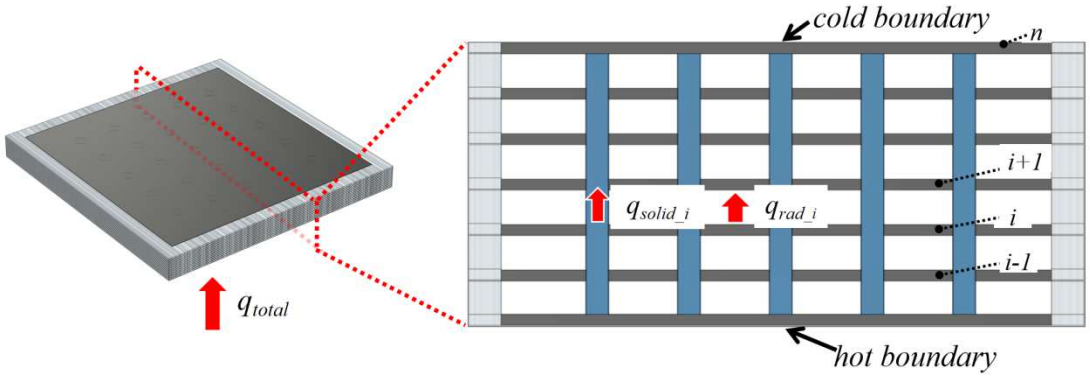


Fig. 4 Heat transfer process by the layer-by-layer model

The total heat flux of the ceramic array LBMLI composed of n layers of reflective screens can be expressed as:

$$q_{total}=q_{total_radiation}+q_{total_solid} \tag{9}$$

where $q_{total_radiation}$ is the radiant heat flux and q_{total_solid} is the thermal conductivity heat flux.

The net radiant heat flux density generated through screen's surface between the i^{th} layer and the $i+1^{st}$ layer of adjacent reflective layers can be expressed as:

$$q_{radiation_i}=\frac{\sigma\left(T_i^4-T_{i+1}^4\right)}{1/\varepsilon_i+1/\varepsilon_{i+1}-1} \tag{10}$$

where T_i and T_{i+1} are the temperature of adjacent reflective screens by i^{th} layer and the $i+1^{st}$ layer surfaces respectively, ε_i and ε_{i+1} are the emissivity of screens by i^{th} layer and the $i+1^{st}$ layer surfaces respectively.

If ceramic array LBMLI is composed of a total of n layers of screens, the emissivity of every screen surfaces is ε, then the radiant heat flux density between all of the adjacent reflective screens can be expressed as:

$$q_{total_radiation}=\frac{\sigma\left(T_1^4-T_n^4\right)}{(n-1)(2/\varepsilon-1)} \tag{11}$$

The heat conduction between the reflective screens is achieved through the ceramic particles. The heat flux conducted by the ceramic dots between the i^{th} layer and the i+ 1^{st} layer of the reflective screens is:

$$q_{solid_i}=\frac{k_{solid}(T_i-T_{i+1})}{d} \tag{12}$$

where k_{solid} is the thermal conductivity of ceramic dots, d is the spacing of the adjacent reflective layers.

For the ceramic array LBMLI composed of a total of n layers of screens, the total heat flux is:

$$q_{total}=\frac{\sigma\left(T_1^4-T_n^4\right)}{(n-1)\left(2/\varepsilon-1\right)}+\frac{k_{solid}(T_1-T_n)}{d\cdot n} \quad (13)$$

For a complete RTPV system, the thermal efficiency by ceramic array LBMLI $\eta_{thermal}$ is expressed as the as the total power $Q_{heat\ power}$ minus the thermal power of the ceramic array LBMLI $Q_{ceramic\ array\ LBMLI}$, and it is the total ratio to the heat source energy $Q_{heat\ power}$, as follows:

$$\eta_{thermal}=1-\frac{Q_{CAMLI_screen}+Q_{CAMLI_frame}}{Q_{heat\ power}} \quad (14)$$

2.4 Compared between the above two models

Results are calculated under the same conditions, including temperature in hot boundary is 1000 ℃, and temperature in cold boundary is 20 ℃. Besides, the thermal conductivity of the ceramic array is assuming as composite material composed with hollow ZrO_2 microspheres, being 0.1 W/m·K[27]. The thermal conductivity of the reflective screen is 143 W/m·K as molybdenum[28] and the emissivity of the reflective screen could be assuming as 0.1[29]. Moreover, assuming that the process of the frame absorbing heat energy is not considered. The power loss results of a 15-layer ceramic array LBMLI by the above two theoretical models is shown in the Fig. 5. Layer-by-layer model does not detailed predict the thermal performance for it assuming that heat conduction power and heat radiation power between adjacent reflective screens is same in each layer. The heat radiation loss between the reflective screens near the hot end is the main factor, while the heat conduction loss is the main factor near the cold end.

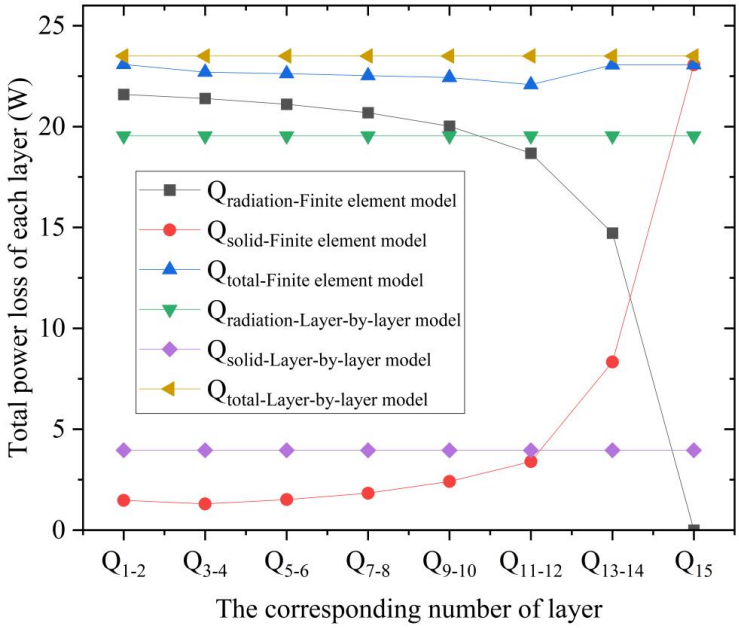


Fig. 5 The total heat power loss in the ceramic array LBMLI's each layer with 9 ceramic dots

Fig. 6 shows the max and min temperature of the different reflective screens. When the screen is close to the hot boundary, the difference between the maximum and minimum values of the reflective screen surface temperature is small. In detail, the maximum temperature of the 3rd layer reflective screen surface is 945.67 ℃, and the minimum temperature is 945.34 ℃, differing by 0.34 ℃. However, the maximum temperature of the surface of the 13th layer of the reflective screen is 428.34 ℃, and the minimum temperature is 420.02℃, differing by 8.32 ℃. By applying the finite element analysis method, the temperature distribution in the LBMLI can be analyzed in detail, then we all use this method to analyze the LBMLI's characteristic.

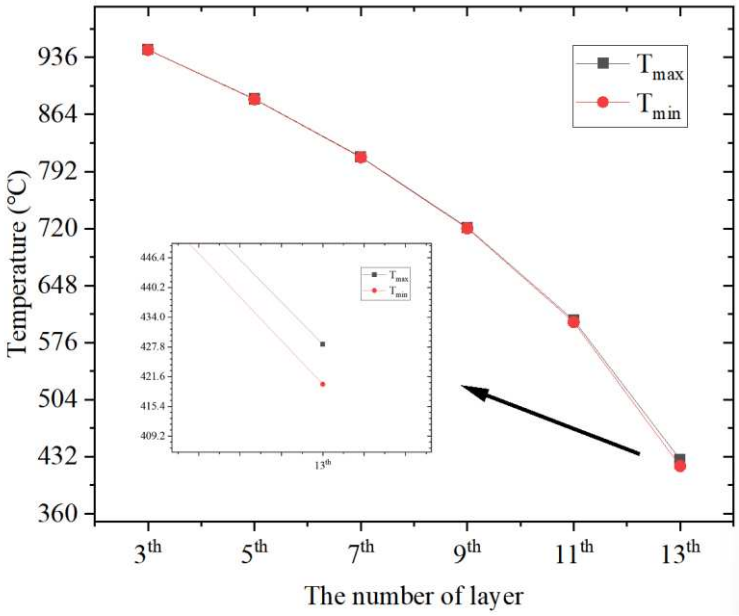


Fig. 6 The temperature of the different reflective screen

3 Ceramic array LBMLI's thermal performance

Ceramic dot arrays with different parameters are simulated and designed to investigate the process of reducing heat loss in ceramic array LBMLI. The influence on the average temperature of ceramic array LBMLI's every reflective screen is analyzed in detail.

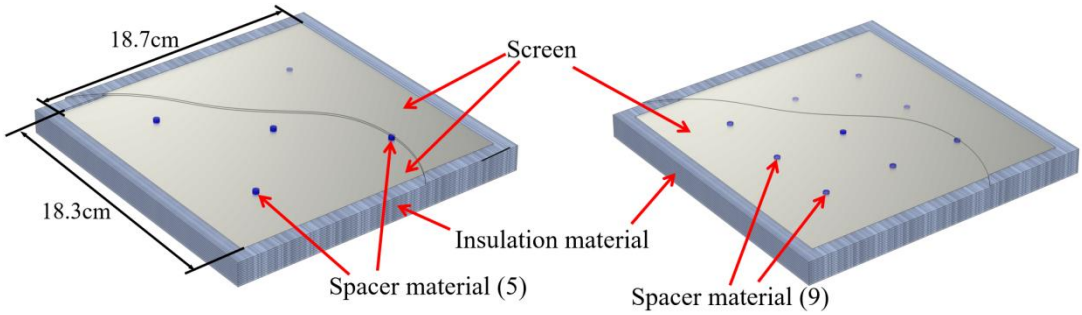


Fig. 7 15-layer ceramic array LBMLI models with ceramic dots. (a) 5 ceramic dots in each screen; (b) 9 ceramic dots in each screen

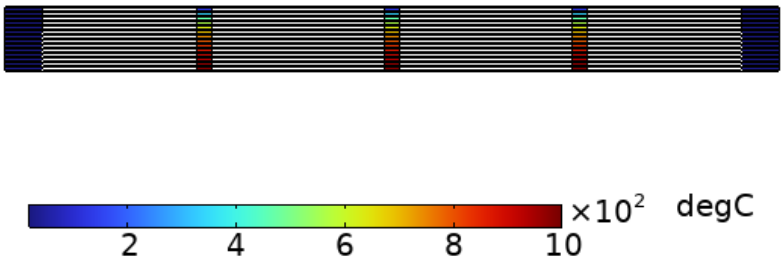


Fig. 8 The cross-sectional temperature distribution (9 ceramic dots in each screen)

Fig. 7 illustrates the ceramic array LBMLI composed of reflective screens with 15 layers, and the spacer materials are designed of two ceramic dot distribution forms, difference lies in the quantity. The ceramic dots are evenly distributed on the surface of the screen to enhance the structural performance. The temperature of each layer of reflective screens inside each structure is calculated as shown in Fig. 8. The distribution structures of the two spacers material structures are analyzed in detail simultaneously under different numbers of layers.

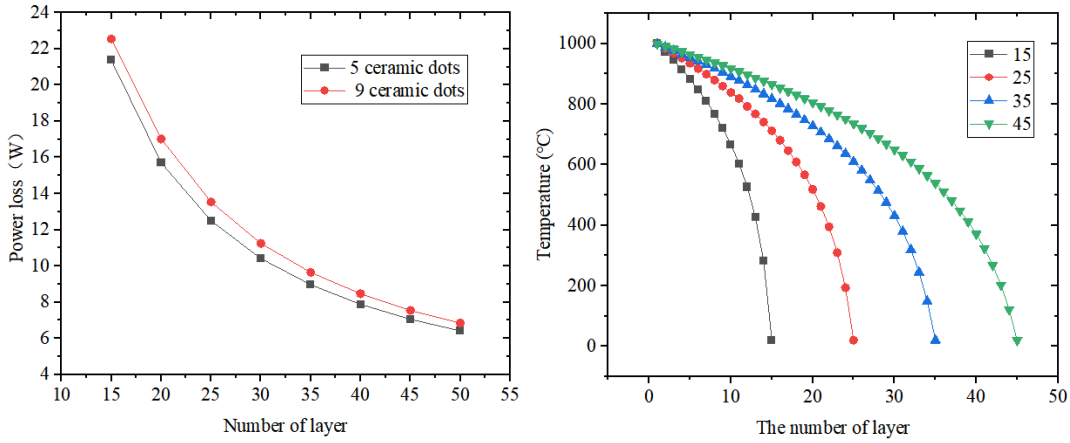


Fig. 9 (a) Power loss vs the number of reflective screen with 5 ceramic dots, and 9 ceramic dots. (b)The reflective screen temperature with 9 ceramic dots.

As shown in the Fig. 9(a), the heat power loss drops sharply with the increase in the number of reflective screens. As the number of layers increased from 15 to 20, the heat power loss significantly decreased from 22.5 W to 17 W. But when the number of layers sets from 45 to 50, the power reduction is less than 2 W. Furthermore, in the Fig. 9(a), when the number of spacer changes from 5 ceramic dots to 9 ceramic dots, the power loss differences is 1.5 W in 15-layer ceramic array LBMLI, that of it is 0.5 W in 45-layer ceramic array LBMLI.

In Fig. 9(b), as the number of reflective screens increases, a greater number of segments of the reflective screens across the entire temperature range. From Equation (9), the thermal radiation flux between the reflective screens decreases. The temperature difference of the first two adjacent screens of the 15-layer ceramic array LBMLI is

24 ℃, while those of them in the 45-layer ceramic array LBMLI is 9 ℃. Results show that the number of layers would influence the thermal power loss and temperature distribution.

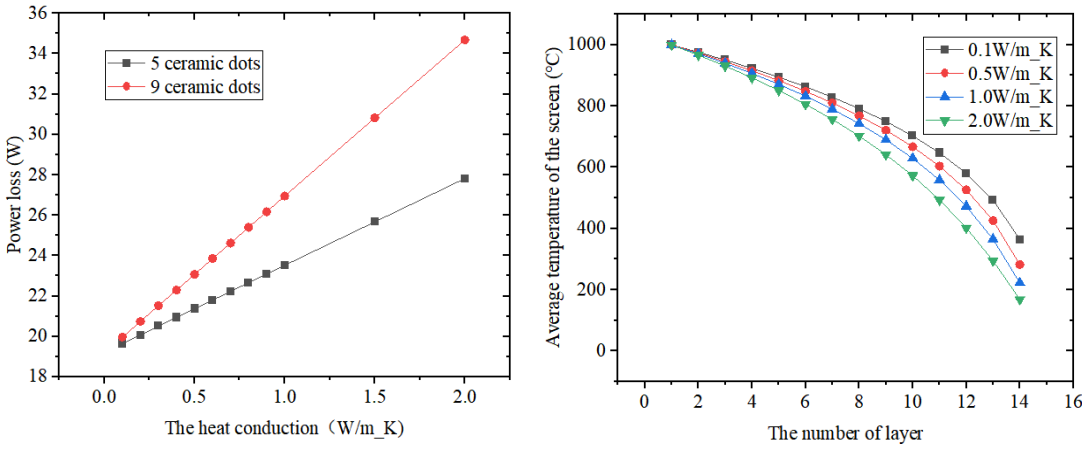


Fig. 10 (a) Power loss vs different thermal conductivity ceramic dots with in 5 and 9 ceramic dots. (b)The reflective screen temperature with 9 ceramic dots.

Fig. 10(a) shows the heat power loss of the ceramic array LBMLI with the different thermal conductivity and number of ceramic dots. The total power loss increases linearly as the thermal conductivity of the spacer material increases. The results shown in Fig. 10(a) is consistent with the prediction by Equation (10).

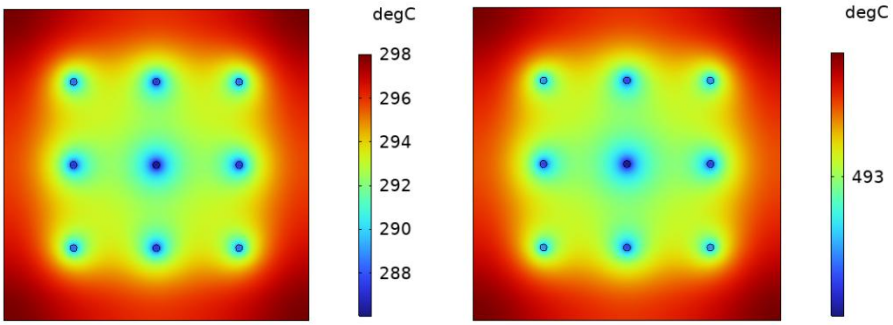


Fig. 11 (a) Temperature of 13th layer as the thermal conductivity is 2.0 W/m·K (b)Temperature of 13th layer as the thermal conductivity is 0.1 W/m·K

As shown in Fig. 10(b), when the thermal conductivity of the ceramic dot spacer material increases, the temperature of the same reflective screen decreases. This indicates that the heat transfer process of the ceramic array LBMLI could be affected by the thermal conductivity of ceramic dot spacer material, then the overall temperature distribution of the internal reflective screen tends to be more linear. When the thermal conductivity is 2.0 W/m·K, the 13th layer's screen temperature is 294.48 ℃ in Fig. 11(a) . When that of the ceramic array LBMLI's spacer materials is 0.1 W/m·K, the screen temperature is higher, change to 493.3 ℃, in Fig. 11(b). Consequently, the solid conduction in ceramic array LBMLI through spacer particles must be considered under the complete contact. If the parameters including the area or the number of the spacer particles are changed, the resulting effect will be similar.

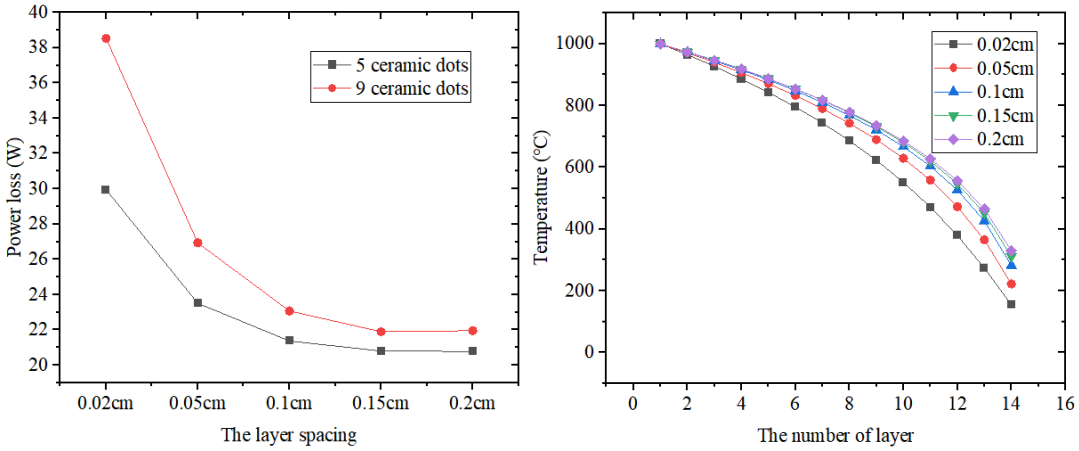


Fig. 12 (a) Power loss vs the layer spacing with 5 ceramic dots, and 9 ceramic dots. (b)The reflective screen temperature with 9 ceramic dots.

To verify the influence of ceramic array LBMLI's spacing, the height of ceramic dots is changed from 0.02 cm to 0.2 cm. As shown in Fig. 12(a), the total heat power loss significantly decreases from 38.52 W to 21.95 W as the layer spacing increases. When the layer spacing is small, the thermal radiation loss between the reflective screens decreases slowly, but the heat conduction power loss significantly increases. The layer spacing between adjacent reflective screens mainly affects the heat conduction effect through the ceramic dots spacer material. A reduction in spacing lead to the decrease of heat transfer path between adjacent reflective screens, and then the heat transfer flux increases. But when the layer spacing exceeds 0.15 cm, the power loss changes slowly.

As shown in Fig. 12(b), when the distance between adjacent reflective screens increases from 0.02 cm to 0.15 cm, the average temperature of the every screen in the ceramic array LBMLI tends to be linear as the layer spacing decreases, it also indicates that the ceramic dots spacer material heat conduction increases due to the layer spacing decreasing. According to the above results, it shows a slightly better performance when the layer spacing is set as 0.1 cm.

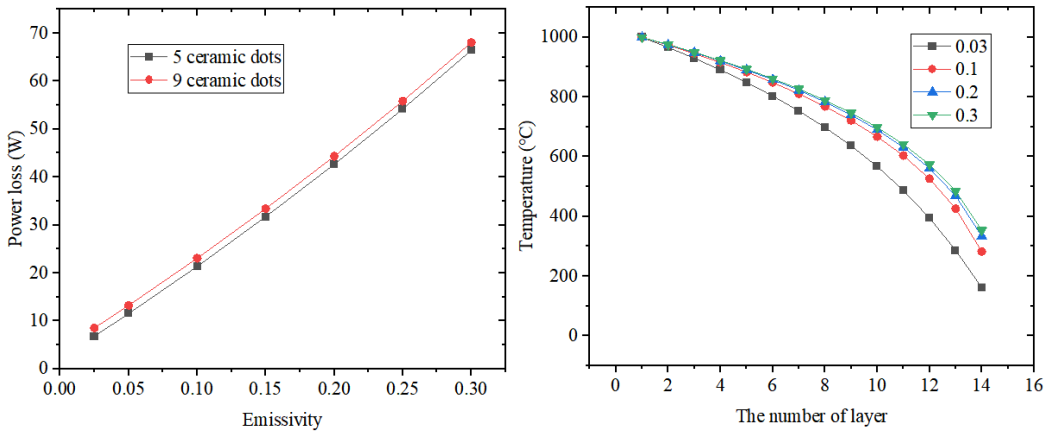


Fig. 13 (a) Power loss vs the emissivity of reflective screens with 5 ceramic dots, and 9 ceramic dots. (b)The reflective screen temperature with 9 ceramic dots.

Fig. 13(a) shows the influence of ceramic array LBMLI's thermal performance of the reflective screens' emissivity. The thermal radiation power loss of the ceramic array LBMLI varies almost linearly with the emissivity of the screens. Emissivity of molybdenum is related to the roughness of its surface. Currently, the roughness of molybdenum in the experimental process can be polished and reach 10 nm, its emissivity is slightly higher than 0.1. As shown in Fig. 13(b), when the emissivity of the reflective screen increases, the temperature distribution inside the reflective screen is affected by the thermal radiation power, and the trend of the temperature change curve increases. The decrease in emissivity of screens lead to the temperature gradient between the reflective screens increases.

Therefore, the physical characteristics of ceramic array LBMLI are as follows: The number of layers of the reflective screen is 15 layers; The spacing of the reflective screens is 0.1 cm. According to the our present RTPV system's structure, the dimensions shown in Fig. 14 should be adopted for the ceramic array LBMLI in this design. The primary limitation of the insulation performance lies in the number of ceramic dots between adjacent screens. The support between adjacent screens within the ceramic array LBMLI is realized through ceramic dots. On the premise of achieving the thermal insulation effect, the number of ceramic dots should be as small as possible to reduce the heat leakage through the ceramic dots. However, the selection of the number of ceramic dot arrays in each screen must take into account the mechanical stability of ceramic array LBMLI.

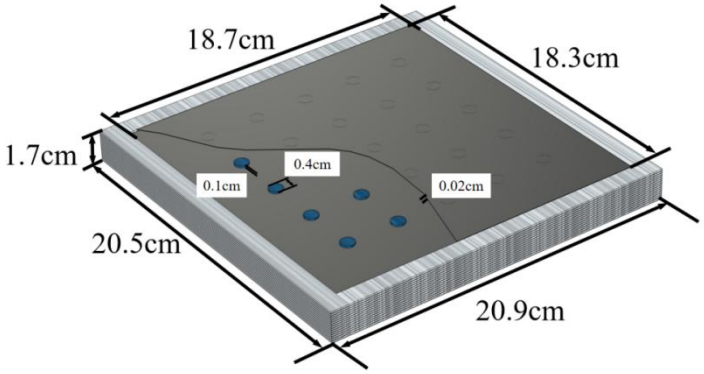


Fig. 14 Size of the ceramic array LBMLI

When the bottom reflective screen is fixed, under the action of the gravitational load, the bending degree of other reflective screen is analyzed. Besides, assuming that the horizontal positions of ceramic dots between layer by layer of the reflective screens are all consistent, and they are complete cylindrical bodies. The mechanical properties of the molybdenum and ZrO_2 ceramic dots in this structure at room temperature, including Young's modulus and Poisson's ratio are listed in Table 1.

Table 1 Material's parameter of Molybdenum and Zirconium oxide

Name	Molybdenum	Zirconium oxide
Young's modulus	329 [GPa]	200 [GPa]
Poisson's ratio	0.31	0.25

The results of displacement magnitudes of the ceramic array LBMLI affected by gravity are shown in Fig. 15, when 4 or 25 ceramic dots are used on each layer of the reflective screen surface. Results show that increasing the number of ceramic dots can significantly reduce the maximum displacement value of the reflective screen's surface bending and displacement at edge position of is the greatest.

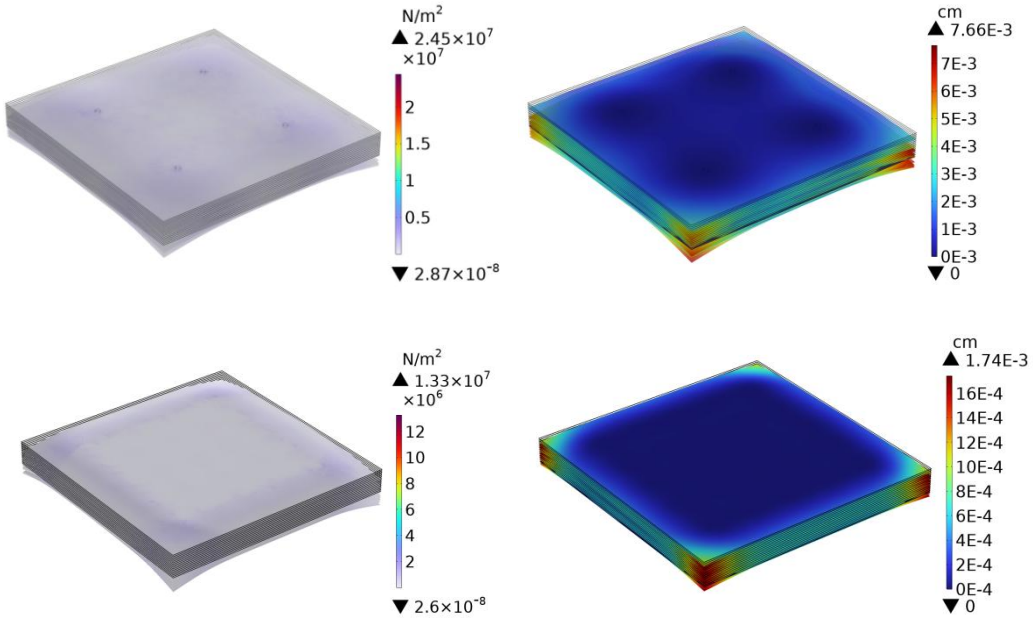


Fig. 15 The mechanical simulated results of ceramic array LBMLI with 4 or 25 ceramic dots.

Fig. 16 shows the bending displacement results of the reflective screens. Assuming that thermal stress is not taken into account, to prevent the adjacent reflective screens from contacting with each other and to ensure the clearance, the maximum bending displacement of the reflective screens should not exceed 0.2 mm. According to the simulated results, if the screen's thickness is 0.2 mm, when the number of spacer material is 4, its distance is 0.0906 mm, and when the number of spacer material is 25, its distance is 0.0174 mm, which can meet the requirement and more safely.

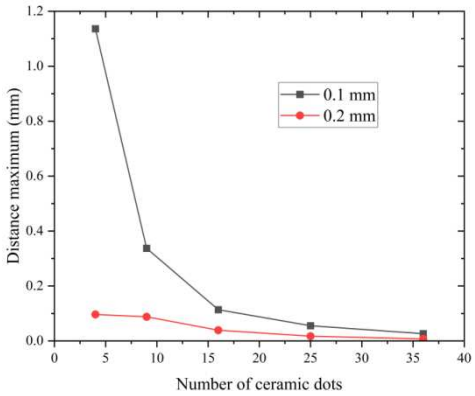


Fig. 16 The distance for a 15-screen ceramic array LBMLI between two different thicknesses of reflective screens.

4 Simulation and analysis of the RTPV with ceramic array LBMLI

4.1 Modeling of the RTPV

Fig. 17 shows the arrangement of the PV cells, the cooling plates, the filter, the emitter and the ceramic array LBMLI around the GPHS heat source in the experimental prototype RTPV system. The surface temperature of the GPHS heat source is over 800 ℃, and there is an optical filter to manage its radiant energy spectrum. The filter reflects unusable radiation back to the heat source while selectively transmitting a narrow band of useful energy to the TPV cells. These cells subsequently convert the transmitted energy into electricity. To maintain optimal performance and prevent overheating, a cooling plate is employed to dissipate excess heat from the PV cells. The cells convert the transmitted energy to electricity, and the cooling plate is used to lower the temperature of the PV cells. The ceramic array LBMLI with molybdenum reflective screens and thermal insulation materials are placed on both the top and bottom of the heat source to prevent heat loss from these two surfaces, and increase the temperature of the heat source and emitter. And the filter and cooling plate are mechanically supported by the ceramic array LBMLI. The total thickness of the ceramic array LBMLIs frame is 1.1 cm, while the height of the reflective screen remains at 0.2 mm. The dimensions of the 15 internal reflection screens are 18.3 cm ×18.7 cm, the spacing between adjacent reflective screens is 0.1 cm. Each ceramic dot has a diameter of 0.4 cm. On each layer of reflective screen, 25 ceramic dots with a thickness of 0.1 cm are arranged to separate adjacent reflective screens.

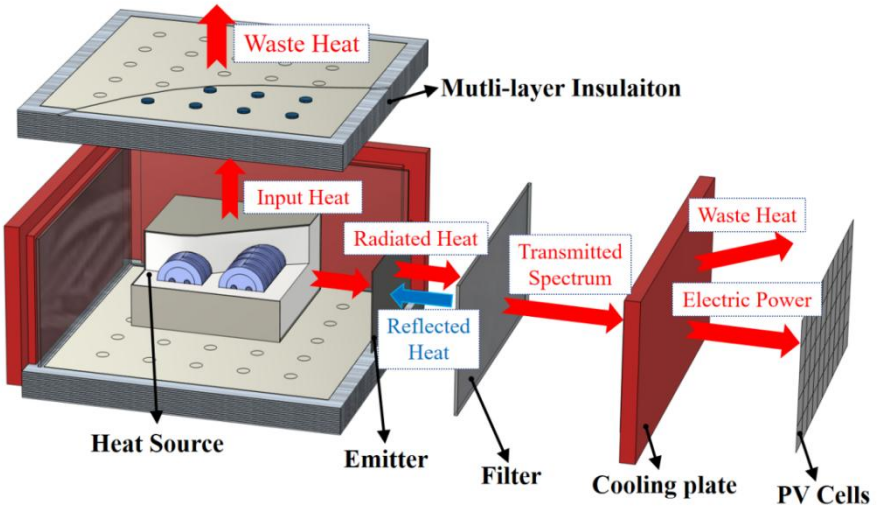


Fig. 17 Arrangement of the structure arrays around a GPHS heat source in the RTPV system

The experimental heat source in the present system is shown in Fig.18 (a), it includes a structure equipped with an electric heating system to replace the GPHS heat source, which can generate a maximum of 250 W of heat using plutonium nuclear fuel. The heat source is composed of silicon carbide spiral tubes, ceramic matrix and tungsten emitter. The length and width are 99 mm and 95 mm respectively, and the height is 55 mm. At the position P as shown in Fig. 18(b), a point T_p is set for measuring

the heat source's temperature. In addition, the heat input power is set within the two silicon carbide spiral tubes, power is conducted to the emitter through heat conduction and generates thermal radiation.

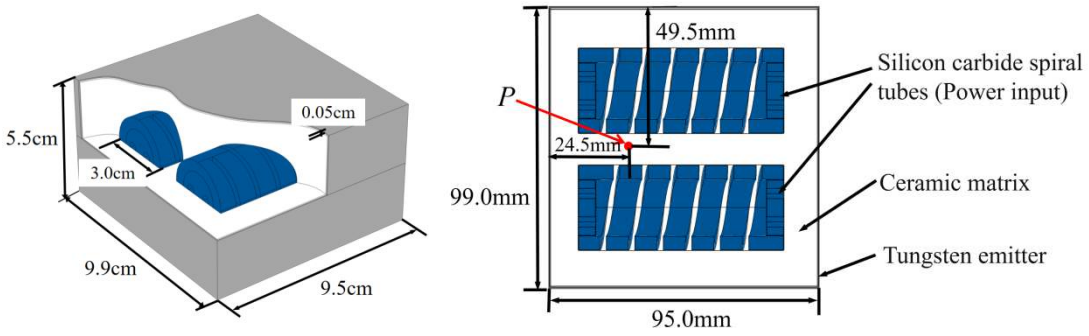


Fig. 18 (a) The size of the heat source; (b) The position of the thermocouple.

Four cooling plates that circulate coolant internally for cooling in the RTPV system are proposed, and the internal coolant is connected through external water pipes. During the calculation process, the surface temperature of the cooling plates is assumed to be set as 20 ℃, and the surface temperature is uniform. The simplified cooling plate model and its dimensions are shown in the Fig. 19(a). Fig. 19(b) shows the process of heat transfer to the cooling plate in the RTPV system. The blue streamlines represent the heat conduction mode to the cooling plate, the red streamlines represent the total heat radiation mode to the cooling plate, and the black streamlines represent the heat radiation mode to the ceramic array LBMLI, including *Q(MLI_frame)* and *Q(MLI_screen)*, The green streamlines represent the heat radiation mode to the environment from ceramic array LBMLI.

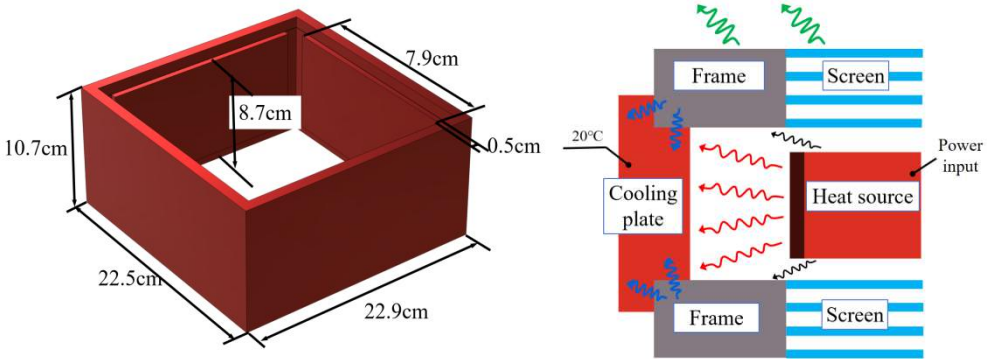


Fig. 19(a) The size of cooling plate; (b) The heat flux in cooling plate.

The corresponding names and parameter of the key materials are shown in Table 2. Fig.20 shows the spectral characteristics emitter, filter, and screen. For the tungsten with a roughness of 10 nm, the spectral emittance has been measured. The two-dimensional photonic crystal is used, which has high transmittivity in the range of 0.8 μm to 1.8 μm, being convertible by the PV cells. The ceramic array LBMLI's screen is molybdenum, polished to a roughness of 10 nm, and the surface emissivity is also shown.

Table 2 Design Parameters for the Radioisotope thermophotovoltaic system

Name	Material	Thermal conductivity (W/m·K)	Emissivity
Heat source_Ceramic	Aluminium oxide	20	0.45
Heat source_Core	Carborundum	31.6	—
Heat source_Emitter	Tungsten	174	Fig. 20
Filter	Glass	1	Fig. 20
Cooling plate	Copper	400	0.05
Ceramic array LBMLI_Screen	Molybdenum	140	Fig. 20
Ceramic array LBMLI_Lattice	Hollow Zirconia Material	0.1	0
Ceramic array LBMLI_Frame material	Aerogel	0.02	0.55

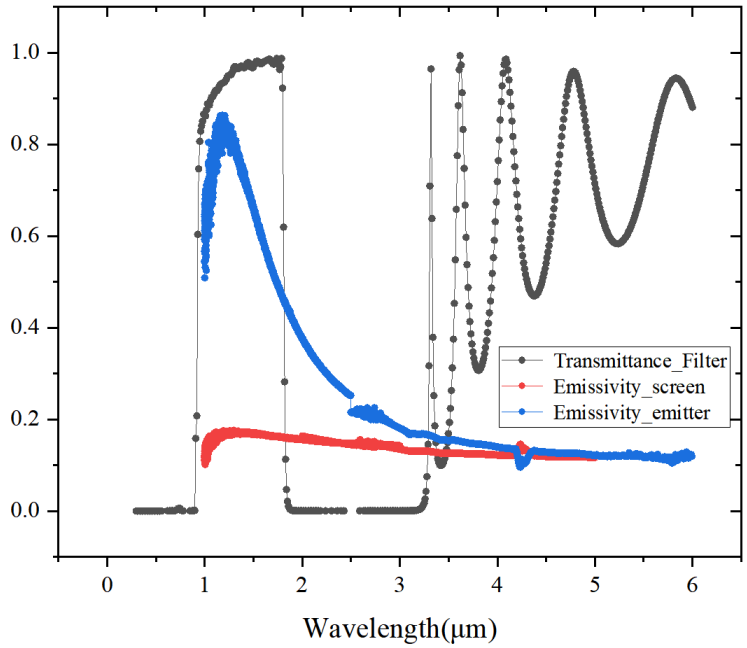


Fig. 20 Spectral characteristics of several materials in the RTPV system

The edge insulation frame of ceramic array LBMLI affects the heat loss, two models are analyzed. The first one is assumed that the heat loss of the frame is not considered (Ideal insulation frame). As shown in Fig. 21(b), for the heat analysis in the RTPV system, the total heat flux q_{total} of ceramic array LBMLI is entirely transferred through the reflective screens in the form of heat radiation. The net heat flow can be expressed with the screen's heat flux (q_{screen}). The second model is to consider the heat flow through the frame insulation material (Actual insulation frame). Part of the heat flow is lost through the cooling plate and the environment. Total heat flow q_{total} through the ceramic array LBMLI is the sum of the reflective screen q_{screen} and frame insulation $q_{insulation}$, and the energy $q_{frame\text{-}i}$ that enters the i^{th} layer of the frame through the reflective screen on the surface of the internal i^{th} layer is in the form of heat radiation.

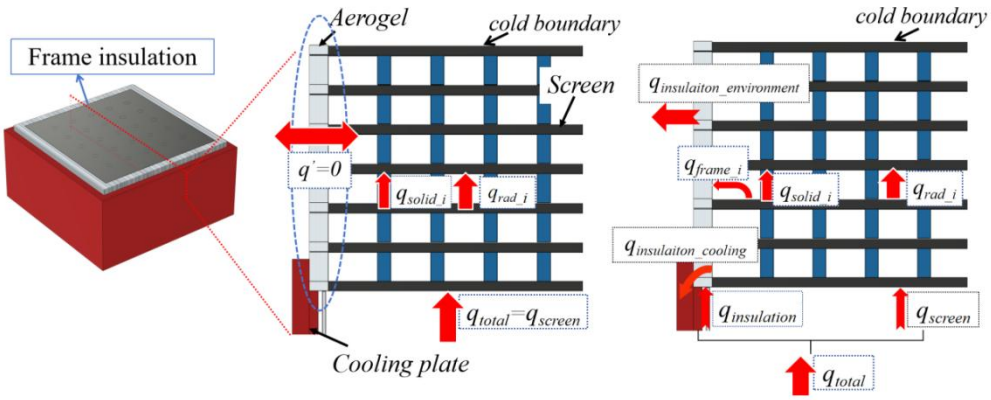


Fig. 21 Illustration of energy flow through ceramic array LBMLI for RTPV system, (b) Assuming the frame is made of ideal frame insulation material (Ideal insulation frame): $q_{insulation} = 0$, (c) Actual frame insulation material (Actual insulation frame): $q_{insulation} \neq 0$

4.2 Estimation of temperature under different input power and edge effects

When the silicon carbide tube of the heat source increases from 25 W to 300 W, the thermal performance calculated results of the RTPV system with ceramic array LBMLI structure are simulated and experimental tested. The prototype RTPV system is tested by using ceramic array LBMLI and reached 1050 ℃ in the heat source. The temperature of the heat source at measurement point P are all shown in Fig. 22. Results show that the ceramic array LBMLI with ideal and insulation materials have different thermal performance on the RTPV system. When considering the ideal frame insulation materials, the temperature of the heat source in the RTPV can reach 1106.3 ℃, while the temperature with the actual frame insulation is 1079.4 ℃. Therefore, the heat loss of the frame cannot be ignored when designing the ceramic array LBMLI in the RTPV system. Additionally, experimental results show that when the heat power is 290.84 W, T_p is 1050 ℃, lower than that of simulation results being 1161.4 ℃ at 300 W by the actual insulation frame.

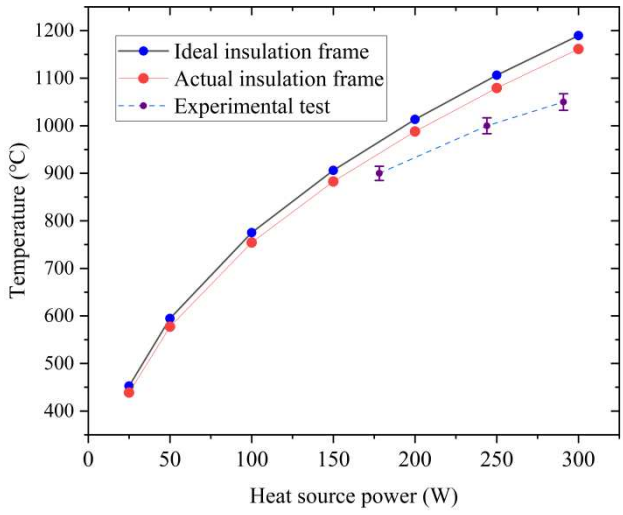


Fig. 22 Relationship between temperature and heat source power in the simulated results.

Furthermore, the cross-sectional temperature distributions are compared in Fig. 23. When the heat source power is 250 W, *P2* in helical silicon carbide elements is 1298.0 ℃ in actual insulation, 1319.7 ℃ in ideal insulation, *P1* in the surface temperature of the heat source is 867.4 ℃ in actual insulation, 900.9 ℃ in ideal insulation. For the RTPV system with the actual insulation, the average temperature of the reflective screen close to the heat source is 688.2 ℃, but the temperature far away the heat source is 137.5 ℃. For the RTPV system with the ideal insulation frame, the average temperature of the reflective screen close to the heat source is 748.8 ℃, but the temperature far away the heat source is 181.6 ℃.

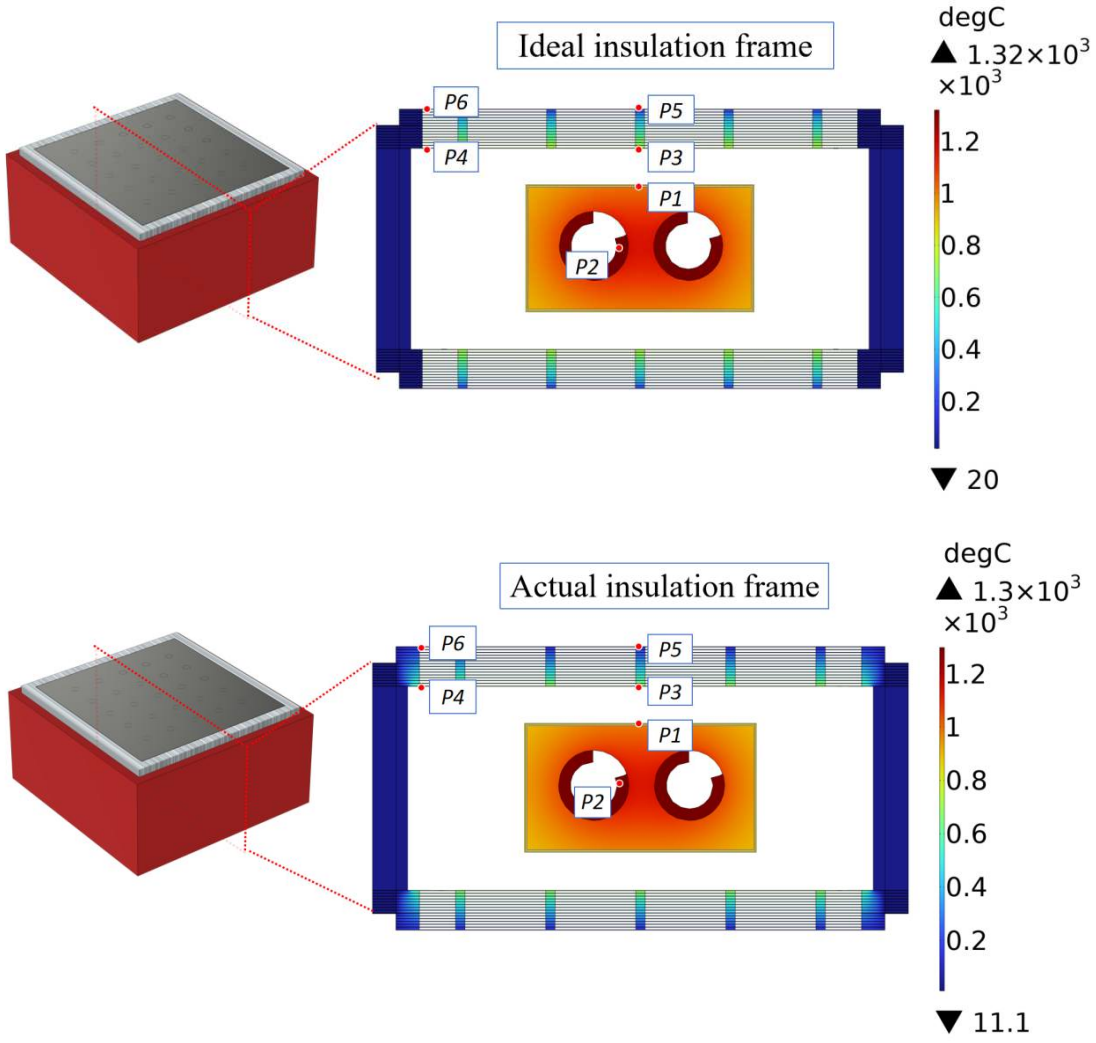


Fig. 23 Cross-sectional temperature distribution of the RTPV system (250 W)

Table 3 Results of the temperature distribution

Position	***P1***	***P2***	***P3***	***P4***	***P5***	***P6***
Ideal insulation frame	900.9	1319.7	771.3	740.9	182.5	181.6
Actual insulation frame	867.4	1298.0	713.4	681.9	118.3	117.8

The heat flow power of various devices in the RTPV system is shown in Table 4. Table 5 shows the thermal efficiency $\eta_{thermal}$ by formula (14). For ideal insulation frame, the heat power loss of MLI are 43.45 W, 173.72 W from the cooling plates and 32.83 W from the others devices. For actual insulation frame, the heat power loss results are 55.05 W from ceramic array LBMLI's screen, 26.30 W from the ceramic array LBMLI's frame insulation materials, 142.59 W from the cooling plate and 26.06 W from the cavity. The frame lead to conduct heat power along the edges of the screens. At the same time, the area of ceramic array LBMLI are approximately four times that of the structure mentioned in the literature by Schock[10]. The power results equivalent obtained is total 79.68 W by 15-layer, which is basically approach three times than the power loss of 60-layer ceramic array LBMLI in the RTPV system studied by Schock as 29.0 W[10], because considering influence of number of screens' layers varying.

Table 4 Heat power loss at the key material

Name	Ideal insulation frame	Actual insulation frame
Q_{MLI_screen} (W)	43.45	55.05
Q_{MLI_frame} (W)	0	26.30
$Q_{cooling\ plate}$ (W)	173.72	142.59
Q_{others} (W)	32.83	26.06

Table 5 Thermal efficiency of the RTPV system

Name	Ideal insulation frame	Actual insulation frame
$\eta_{thermal}$	69.5 %	57.0 %

4.3. Thermal analyze of the RTPV considering optical cavity size

To analyze the influence of the cavity size on the thermal efficiency and temperature, we adjust the devices' size in the system except for the heat source in proportion. The heat source has a power input of 250 W, and the proportion for the design in the lateral two dimensions is named as *XY_size*. *XY_size* depends on the reduction of the MLI's size by 2 cm, 4 cm, 6 cm and 8 cm each. Although it may not be as nice as the predicted values from the complete theoretical modeling, by this method the thermal performance of systems with different cavity sizes can be obtained with less simulation effort. Fig. 24(a)-(c) respectively illustrate three typical size configurations.

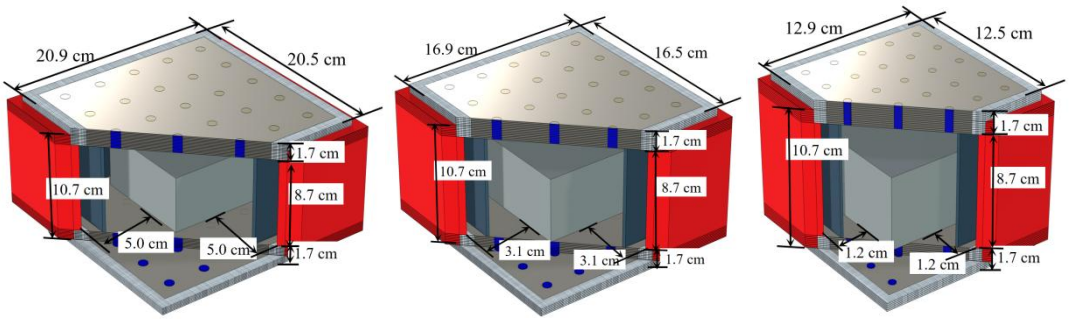


Fig. 24 Three typical size configurations.

As shown in Fig. 25, the cavity structure of the RTPV system is designed in different configurations, which will cause changes in the temperature of the heat source. When the cavity size is reduced, the temperature of T_p inside the heat source increases from 1106.3 ℃ to 1195.2 ℃ by the ideal insulation frame and 1079.4 ℃ to 1159.9 ℃ by the actual insulation frame. This is because as the size of the cavity decreases , the area of the MLI at both ends and the area of the cooling plates decreases, it leads the loss of waste heat absorbed by the system reducing.

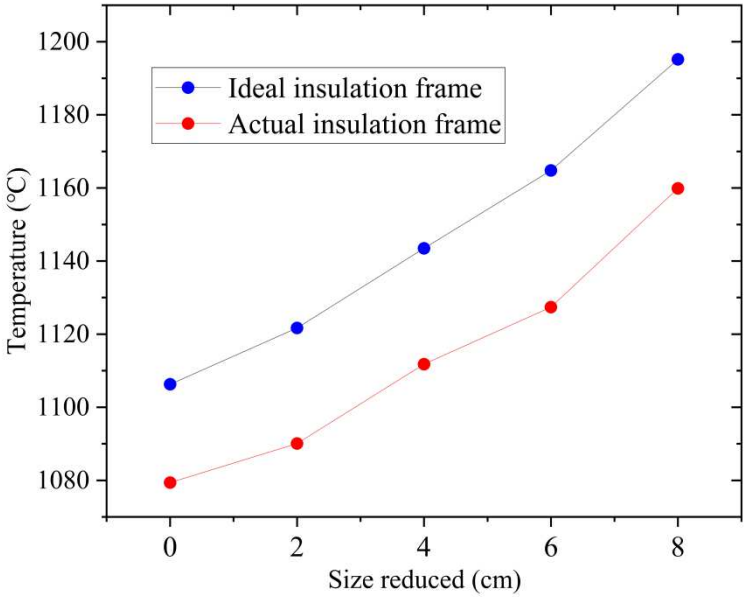


Fig. 25 Temperature of heat source when *XY_size* ranges from 0 cm to 8 cm.

Furthermore, the temperature distribution of the emitter on the heat source surface is also an important factor in evaluating the thermal performance of the RTPV system. As shown in Fig. 26, when the size of the cavity in the lateral directions decreases, the temperature of the front surface of the heat emitter on the heat source surface by actual frame situation becomes more concentrated in the central area, and the overall temperature has become even more uneven, which may result in difference of the radiation spectral efficiency of the effective band on the heat source surface, and the change of thermal radiation spectral irradiation effect. For example, when the *XY_size* is 8 cm, there is a clear concentration of temperature distribution and the maximum

value is 944.76 ℃, the average temperature of the surface is 939.62 ℃. But when it is not changed, the maximum value is 845.41 ℃ and the average temperature is 838.80 ℃.

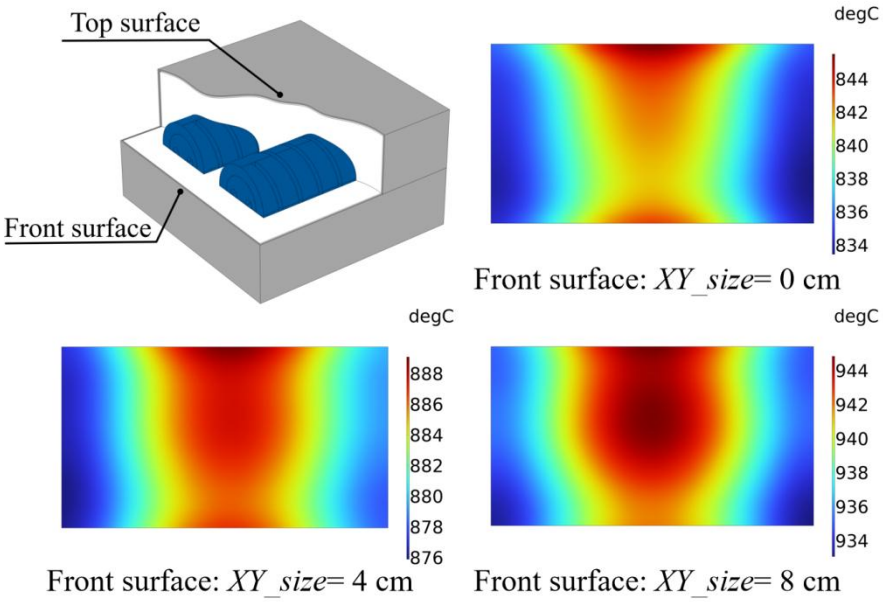


Fig. 26 Temperature distribution of heat source surface by actual insulation frame.

The parameters of the cavity size also affect the situation of each device absorbing thermal power in the RTPV system. *XY_size* of different cavity structures respectively affect the thermal efficiency of the RTPV system radiation absorption as shown in Fig. 27. When *XY_size* increases to 8 cm, the proportion of thermal energy efficiency from the surface of the cooling plate increases to 72.1% by the ideal insulation frame and 60.2% by the actual insulation frame. Result shows that reducing the geometric size of the RTPV system can lead much more thermal energy to be utilized.

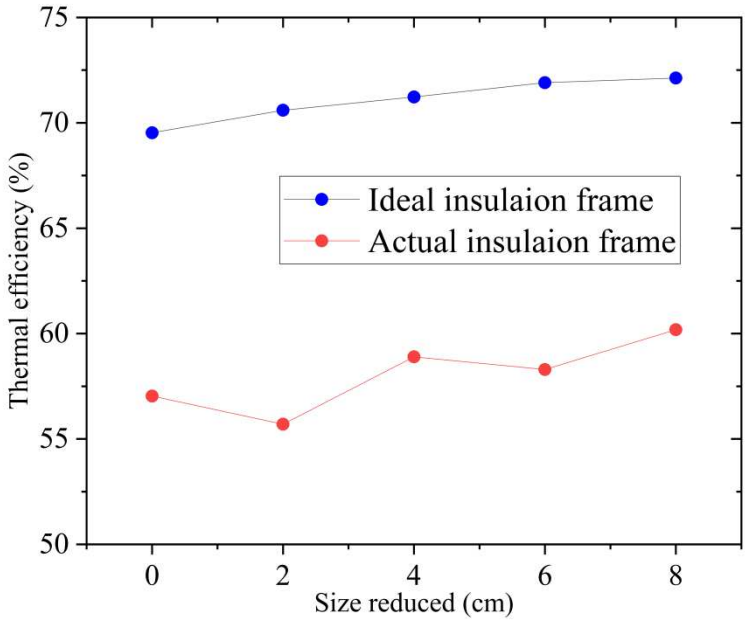


Fig. 27 Thermal efficiency of the RTPV system.

5 Conclusion

An RTPV system with hollow ZrO_2 ceramic array LBMLI is proposed, key parameters such as numbers of screens, number and thermal conductivity of ceramic array-type, spacing and emissivity of the reflective screen are analyzed. At hollow ZrO_2 ceramic array LBMLI of 9 dots' ceramic array, among the height of spacing of each screen increasing from 0.02 cm to 0.2 cm, the total heat power loss decreases from 38.52 W to 29.95 W, but when the height exceeds 0.15 cm, the power loss changes slowly, so we set as 0.1 cm. Among layers' number from 15 to 50, the heat loss exhibits from 22.5 W to 6.8 W. Then, by reducing the emissivity from 0.1 to 0.025, the heat loss is almost linearly reduced to 8.5 W.

Considering the mechanical stability, 25 dots' ceramic array LBMLI with a 15-layer reflective molybdenum screens and roughness as 10 nm is proposed in the RTPV system. Through theoretical modeling, the heat power loss by different devices, the system's thermal efficiency by ceramic array LBMLI, temperature of the heat source, and cross-sectional temperature distribution are analyzed. If the heat loss from the frame is not taken into account, the temperature of the heat source reaches 1106.3 ℃ and ŋthermal is 69.5%. When it is considered, the temperature of the heat source is 1079.4 ℃, and ŋthermal is 57.0%. Then, considering optical cavity size, when reducing the lateral two dimensions of ceramic array LBMLI by 2, 4, 6 and 8 cm each, temperature of the heat source center change to 1090.1 ℃, 1111.8 ℃, 1127.4 ℃, and 1159.9℃ when not considering insulation frame heat loss, and the system's thermal efficiency increases.

Acknowledgments

This work was supported by Ling Chuang Research Project of China National Nuclear Corporation (CNNC-LCKY-2024-076), the Fundamental Research Funds for the Central Universities, grant No. lzujbky-2023-stlt01, and by the National Natural Science Foundation of China, Grants No. U20B2008.

[1] Kai Liu, Yunpeng Liu, Zhiheng Xu, Zhengrong Zhang, Zicheng Yuan, Xiao Guo, Zhangang Jin, Xiaobin Tang, Experimental prototype and simulation optimization of micro-radial milliwatt-power radioisotope thermoelectric generator, Applied Thermal Engineering, Volume 125, 2017, Pages 425-431, ISSN 1359-4311, https://doi.org/10.1016/j.applthermaleng.2017.07.022.

[2] Christopher J. Crowley, Nabil A. Elkouh, Susan Murray, Donald L. Chubb; Thermophotovoltaic Converter Performance for Radioisotope Power Systems. AIP Conf. Proc. 6 February 2005; 746 (1): 601–614. https://doi.org/10.1063/1.1867178.

[3] Ji Qi, Xuejian Wang, Decao Yang, Gongping Li, Feasibility study on radioisotope-powered thermophotovoltaic/thermoelectric hybrid power generation system used in deep-sea: From design to experiment, Applied Energy, Volume 358, 2024, 122604, ISSN 0306-2619, https://doi.org/10.1016/j.apenergy.2023.122604.

[4] Youhong Liu, Yingzeng Zhang, Qingpei Xiang, Fanhua Hao, Qi An, Haodong Chen, Comprehensive modeling and parametric analysis of Multi-Mission Radioisotope Thermoelectric Generator, Applied Thermal Engineering, Volume 219, Part A, 2023, 119447, ISSN 1359-4311, https://doi.org/10.1016/j.applthermaleng.2022.119447.

[5] WILT D, CHUBB D, WOLFORD D, et al. Thermophotovoltaics for Space Power Applications [Z]. AIP Conference Proceedings. 2007: 335-345. DOI: 10.1063/1.2711751.

[6] Hongyang Jia, Zhiheng Xu, Chao Chen, Xiaobin Tang, A 30-year radioisotope thermophotovoltaic system with a 100-watt output based on 500 W general purpose heat source, Applied Thermal Engineering, Volume 280, Part 2, 2025, 128087, ISSN 1359-4311, https://doi.org/10.1016/j.applthermaleng.2025.128087.

[7] Bohui Huang, Hucheng Wang, Shuming Liu, Hongyi Luo, Xiaoxu Bian, Yan Wang, Zhi peng Ru, Zhiyang Wang, Jianxiong Shao, Aixiang Yang, Ximeng Chen, Dingjun Zhu, Numerical study of temperature distribution and performance optimization of radioisotope thermophotovoltaic system, Case Studies in Thermal Engineering, Volume 75, 2025, 107274, ISSN 2214-157X, https://doi.org/10.1016/j.csite.2025.107274.

[8] WANG H, TANG X, LIU Y, et al. Thermal Emission‐Enhanced and Optically Modulated Radioisotope Thermophotovoltaic Generators [J]. Energy Technology, 2019, 8(3). https://doi.org/10.1002/ente.201901170.

[9] Junghun Lee, Seongjae Cheon, Sergi Hong, Youngsuk Nam, A radioisotope thermophotovoltaic converter with nanophotonic emitters and filters, International Journal of Heat and Mass Transfer, Volume 108, Part A, 2017, Pages 1115-1125, ISSN 0017-9310, https://doi.org/10.1016/j.ijheatmasstransfer.2016.12.049.

[10] KOUDELKA R D. Radioisotope Micropower System Using Thermophotovoltaic Energy Conversion [Z]. AIP Conference Proceedings. 2006: 545-51. DOI: 10.1063/1.2169233.

[11] SCHOCK A, MUKUNDA M, OR C, et al. Analysis, optimization, and assessment of radioisotope thermophotovoltaic system design for an illustrative space mission [Z]. AIP Conference Proceedings. 1995: 331-56. DOI: 10.1063/1.47044.

[12] Ding, Y.; Shao, D.; Jin, S.; Yu, M.; Wang, Y.; Jiang, L. Numerical Study on Composite Multilayer Insulation Material for Liquid Hydrogen Storage. Coatings 2024, 14, 1417. https://doi.org/10.3390/coatings14111417.

[13] JI T, ZHANG R, SUNDEN B, et al. Investigation on thermal performance of high temperature multilayer insulations for hypersonic vehicles under aerodynamic heating condition [Z]. Applied Thermal Engineering. 2014: 957-965. DOI: 10.1016/j.applthermaleng.2014.06.014.

[14] CHEN M, LI Q, ZHANG P. Theoretical and experimental study on a compound insulation system for high temperature applications [J]. Applied Thermal Engineering, 2022, 210. https://doi.org/10.1016/j.applthermaleng.2022.118318.

[15] MIYAKITA T, HATAKENAKA R, SUGITA H, et al. Development of a new multi-layer insulation blanket with non-interlayer-contact spacer for space cryogenic mission [J]. Cryogenics, 2014, 64: 112-20. https://doi.org/10.1016/j.cryogenics.2014.04.008.

[16] HATAKENAKA R, TAKESHI M, SUGITA H, et al. Thermal Performance and Practical Utility of a MLI Blanket using Plastic Pins for Space Use [Z]. 43rd International Conference on Environmental Systems. 2013. DOI: 10.2514/6.2013-3503.

[17] S.A. Dye, W.L. Johnson, D.W. Plachta, G.L. Mills, L. Buchanan, A.B. Kopelove, nDesign, fabrication and test of Load Bearing multilayer insulation to support a broad area cooled, Cryogenics, Volume 64, 2014, Pages 135-140, ISSN 0011-2275, https://doi.org/10.1016/j.cryogenics.2014.06.001.

[18] Xiaoqi Zhou, Dingning Li, Junjie Zhang, Xin Wang, Peter Fisher, Yixin Sun, Shihe Pan, Shipei Zhang, Lin Qiu, Xiawa Wang, Modeling and implementation of multilayer insulation for small-scale ultrahigh temperature systems, Applied Thermal Engineering, Volume 245, 2024, 122838, ISSN 1359-4311, https://doi.org/10.1016/j.applthermaleng.2024.122838.

[19] HUANG C, ZHANG Y. Calculation of high-temperature insulation parameters and heat transfer behaviors of multilayer insulation by inverse problems method [J]. Chinese Journal of Aeronautics, 2014, 27(4): 791-796. DOI: 10.1016/j.cja.2014.03.007.

[20] CHEN M, ZHANG P, LI Q. Design and heat transfer analysis of a compound multi-layer insulations for use in high temperature cylinder thermal protection systems [J]. Science China Technological Sciences, 2018, 61(7): 994-1002. DOI:10.1007/S11431-017-9250-X.

[21] SCHOCK A, EL-GENK M S, HOOVER M D. Radioisotope Stirling Generator Options for Pluto Fast Flyby Mission [Z]. AIP Conference Proceedings. 1994: 345-58.10.1063/1.2950201.

[22] SU Sheng, AI Sufen, QIU Jiawen, SONG Xin, TIAN Dai, MA Bin, CAO Yaru. Preparation and Thermal Performance Study of Multilayer Insulation in RTPV for Deep Space Exploration[J]. Journal of Deep Space Exploration, 2024, 11(5): 462-468. DOI: 10.15982/j.issn.2096-9287.2024.20230133.

[23] DYE S A, JOHNSON W L, PLACHTA D W, et al. Design, fabrication and test of Load Bearing multilayer insulation to support a broad area cooled shield [J]. Cryogenics, 2014, 64: 135-140. DOI: 10.1016/j.cryogenics.2014.06.001

[24] LI P, CHENG H. Thermal analysis and performance study for multilayer perforated insulation material used in space [J]. Applied Thermal Engineering, 2006, 26(16): 2020-2026. DOI: 10.1016/j.applthermaleng.2006.01.004

[25] Xiawa Wang, Walker Chan, Veronika Stelmakh, Ivan Celanovic, Peter Fisher, Toward high performance radioisotope thermophotovoltaic systems using spectral control, Nuclear Instruments and Methods in Physics Research Section A: Accelerators, Spectrometers, Detectors and Associated Equipment, Volume 838, 2016, Pages 28-32, ISSN 0168-9002, https://doi.org/10.1016/j.nima.2016.09.028.

[26] A. HEDAYAT L J H, AND T. BROWN. Analytical modeling of variable density multilayer insulation for cryogenic storage [J]. AIP Conference Proceedings 613, 2002: 1557-1564. DOI: 10.1063/1.1472190

[27] G. Can Tatlisu, Cem Aciksari, Serdar Celebi, Servet Turan, Developing a hollow glass microsphere/geopolymer thermal insulation composite for hot metal surface coating, Ceramics International, Volume 48, Issue 9, 2022, Pages 11924-11939, ISSN 0272-8842, https://doi.org/10.1016/j.ceramint.2022.01.042

[28] Lihua Guo, Xiyang Liu, Jinpeng Zhang, Hongbang Zhang, Xiaokun Gu, Linyuan Lu, Haibing Zhang, Jinwei Zhan, Assessment of thermal conductivity in rolled pure molybdenum after ultra-high temperature exposure via frequency-domain thermoreflectance, International Journal of Refractory Metals and Hard Materials, Volume 134, 2026, 107451, ISSN 0263-4368, https://doi.org/10.1016/j.ijrmhm.2025.107451.

[29] Baizhen He, Aixiang Yang, Zhixuan Lei, Zhiyang Wang, Shuming Liu, Kai Yao, Zhuo Leng, Jianxiong Shao, Chengzhi Han, Dai Tian, Dingjun Zhu, Ximeng Chen, Influence of roughness and temperature on the emissivity of molybdenum in RTPV system, Materials Today Communications, Volume 40, 2024, 110102, ISSN 2352-4928, https://doi.org/10.1016/j.mtcomm.2024.110102.